Acoustic properties of air-saturated porous materials containing dead-end porosity

Thomas Dupont, Philippe Leclaire, Olivier Sicot, Xiao-Lu Gong, Raymond Panneton

Acoustic properties of air-saturated porous materials containing dead-end porosity

T. Dupont,[1,a)] P. Leclaire,[1,b)] O. Sicot,[1] X. L. Gong,[2] and R. Panneton[3,c)]
[1]*LRMA - DRIVE, Université de Bourgogne, 49 rue Mademoiselle Bourgeois, 58027 Nevers cedex, France*
[2]*LASMIS, ICD, UTT, UMR CNRS STMR 6279, 10010 Troyes, France*
[3]*GAUS, Department of Mechanical Engineering, University de Sherbrooke, Sherbrooke, Quebec J1K 2R1, Canada*

This study examines the acoustic properties of materials with complex micro-geometry containing partially open or dead-end (DE) porosity. One of these kinds of materials can be obtained from dissolving salt grains embedded in a solid metal matrix with the help of water. The solid matrix is obtained after the metal, in liquid form, has invaded the granular material formed by the salt particles at negative pressure and high temperature, and after cooling and solidification of the metal. Comparisons between theoretical and experimental results show that the classical Johnson-Champoux-Allard model does not quite accurately predict the acoustic behavior. These results suggest that the assumptions of the Biot theory may not all be fulfilled and that cavity resonators and dead ends can be present in the material. The first part of the study proposes a simple model to account for this geometry. Based upon this model, two acoustic transfer matrices are developed: one for non-symmetric and one for symmetric dead-end porous elements. It is thought that this model can be used to study the acoustic absorption and sound transmission properties of the type of material previously described. In the second part, a series of simplified samples are proposed and tested with a three-microphone impedance tube to validate the exposed model. Finally, the third part compares the predictions of the exposed model to the impedance tube results on a real aluminum foam sample containing dead-end pores. These first results are encouraging and show that this simple model also provides a good prediction for these materials with more complicated microstructure.

I. INTRODUCTION

Air-saturated porous metals such as porous aluminum may be used in numerous applications such as thermal exchangers or shock absorbers in the automobile and aircraft industries. These materials also exhibit interesting acoustic properties. In many applications, they can withstand fairly high temperatures, they can be used in hostile environments (fluid projection and flames), and they are durable and stable in time.

The metal foam obtained following the fabrication process[1] depicted in Fig. 1 is provided the motivation for the present work. In this process, melted aluminum is poured into a container filled with salt grains. The melting temperature of aluminum is 660 °C while that of sodium chloride (NaCl) is 801 °C. Melted aluminum can therefore fill the interstitial spaces between the solid grains. A negative pressure suction is applied in order to facilitate the flow. The grain size distribution can be controlled by successive sieving of the salt grains. After the metal has cooled down, the sample is cut and plunged into water to dissolve the sodium chloride. Then the sample is dried, air replaces the space formerly occupied by the solid grains, and the sample porous metal is created. Figure 2 shows aluminum foam resulting from this fabrication process.

At first sight, the observation of the microstructure and characteristic size of the pores suggests that an equivalent fluid model is well adapted to study the acoustic properties of the resulting foam. In the past, equivalent fluid models have been derived to describe the acoustic wave propagation in rigid-frame open-cell porous media saturated by air.[2] The model used in the present work is that of Johnson-Champoux-Allard. This phenomenological model is accurate and has been successfully applied to sound absorbing materials such as polyurethane foams or fibrous materials.[2–4]

In this article, it is experimentally shown that a classical equivalent fluid model is not as accurate as expected for the studied metallic foams: it appears that the requirement that the pore be "interconnected between them and the surrounding medium" implicitly means that the fluid can flow in all pores and this last condition is not fulfilled in dead ends. In particular, a closer look at the microstructure (Fig. 2) seems to show that some pores are only connected to the exterior by one end. Observation using three-dimensional pictures obtained by a micro-tomography approach confirms the presence of dead-end porosity in these metallic foams.

As summarized in Fig. 3, the hydrogeology scientist distinguishes different kinds of porosities:[5,6]

- Total porosity is defined as the ratio between the air volume (volume without material) and the total volume of the

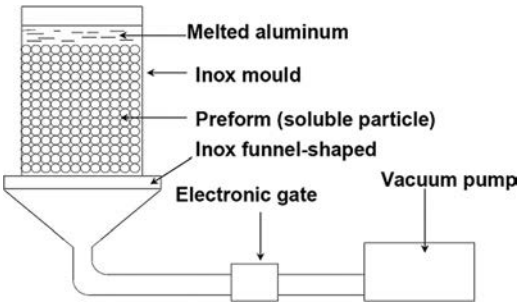

FIG. 1. Principle of the making of aluminum foams (Ref. 1).

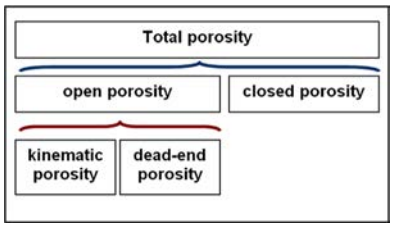

FIG. 3. (Color online) Illustration showing different porosity levels. The kinematic porosity will be referred to as the Biot porosity for the remainder of this paper.

sample in a homogeneous area (representative sample). This porosity includes closed and open porosities.

- Closed porosity (also called residual porosity) represents the cells that are completely closed (not interconnected with others cells). In the rigid frame approach these cells do not influence the acoustical behavior of material.
- Open porosity (also called connected porosity) is defined as the ratio of interconnected pores to the bulk volume of the porous material. This is the ratio between the interconnected open volume and the total volume of the sample. The open volume includes the "mobile volume" of saturation water released under the effect of complete drainage and the "immobile volume" in the connected pore. This open porosity includes kinematic and dead end porosities.
- Kinematic porosity (also called effective porosity or Biot porosity) is related to the displacement of water moving in a permeable medium. It is equivalent to the ratio of the volume of the interstices actually traversed by moving water and the total volume of the medium. The kinematic porosity is the one used in the Biot model and is therefore referred to as the "Biot porosity" for the remainder of this paper. The kinematic porosity can be approximated by drainage porosity, which is defined as the ratio of the volume of water drained by gravity from a saturated representative sample to the total volume of the sample.
- Dead-end porosity (that can also be referred to as "ink bottle porosity") is defined as the ratio of the volume of non-moving water in closed cells to the bulk volume of the porous material; it represents the cells that, although connected to another cell and to the exterior at one end, remain closed at the other end. Bear,[7] who in 1979 worked on interconnected pore space, stated that the porous medium contains dead-end pores, corresponds to material which partially contains pores or channels with only a narrow single connection to the interconnected pore space, so that almost no flow occurs through them. This porosity is referred to as "DE porosity" for the remainder of this paper.

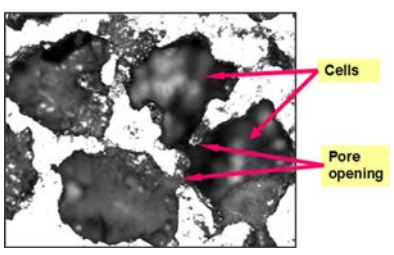

FIG. 2. (Color online) Microstructure of the porous metallic foam (Ref. 1).

The experimental approach of Fatt[8] noted that the DE pore volume may alter transient fluid flow or diffusion behavior. Goodknight[9] proposed identifying the DE volume as continuously distributed equivalent sources. Goodknight proposed analogous equations to describe non-steady-state diffusion through fluid contained in the porous material with DE pores (with neck opening). They proposed an additional source term in the pressure transient equation for homogeneous and isotropic media. Rose[10] discussed this approach and claimed that the additional source had to be more complex: he noted that in most similar cases with this kind of media there was some microscopically inhomogeneous distribution of DE porosity in the material. Rose proposed an analog system with a network of interconnected resistors with a capacitor at the mesh points. The DE pores were represented by capacitors connected to the mesh points through high resistance elements. To characterize the transient of mass equation, they proposed measuring the resistance-capacitance time-constant of the system.

Similarly, Goodknight and Fatt[11] studied the diffusion time-lag in porous media with the DE volume. The time-lag was found with the curve of mass transport against the time delay in achieving steady-state transport. The non-steady state diffusion-equation was solved for a system with the DE pore volume. The model and experimental results showed that the time-lag in a system containing DE pores was influenced by the total pore volume and not by the resistance to flow between the flow channels and the DE pores.

Fatt[12] proposed a network study on the influence of the DE porosity on the relative permeability for a material with simultaneous flow of two or more fluid phases (for example: air-water or air-water-oil). In this network study, the DE pores are created in a classical porous media (or soil) when several liquids flow through the media. He observed that the non-wetting phase relative permeability (air and oil) is strongly influenced by the fraction of the fluid trapped in the DE pores. By contrast, the DE pores do not influence the wetting phase relative permeability (water). He noted that there was no experimental data on real porous material that could verify this prediction. However, he proposed the use of Handy's experiment method (the two-tracer miscible) that uses a fast diffusing and slow diffusing tracer.

Gibb[13] presented a study that documented the laboratory technique for measuring the kinematic porosity of fine-

grained soils. Three soil kinematic porosity measurement methods were discussed: the tracer method, Jacob's method, and the seismic tomography method. Gibb chose to use the tracer method. This approach is based on the travel time measurement through the media. Migration or flow through a porous media can be evaluated by means of tracers. These techniques are difficult to use, given the problems with travel time involved, and are not well adapted to all porous media. This study showed important experimental errors; the kinematic porosity was measured equal to or greater than that calculated for total porosity. Zwikker and Kosten[6] considered cylindrical pores bearing lateral cavities in a rigid solid and assumed qualitatively that, "Notwithstanding the application of a pressure gradient, the air in the lateral cavity remains largely at rest," and that since "the pressure-gradient only succeeds in accelerating the air in the main pore, leaving the air in the side hole at rest," only a porosity correction should be applied. Qian[14] noted that DE pores can slow the particle transport. Therefore, to model the solute transport they proposed the use of an advection-dispersion equation with retardation. In the biophysical domain, Hrabe[15] proposed a model of effective diffusion and tortuosity in the extracellular space of the brain. The model is based on a volume-averaging procedure to obtain a general expression for effective diffusion. In this neurobiological application, the tortuosity is deduced by the square root of the ratio of the effective and free diffusion coefficients. The study used an approximation with a number of regular and randomized 2D and 3D geometries. It noted that "for sufficiently long diffusion times, the DE pore's effects are similar as the case with extra channels were added in a direction perpendicular to the macroscopic diffusion flow." It showed that the "addition of DE pores alters diffusion and increases tortuosity in proportion to the square root of enlarged total extracellular volume fraction." Chevillote *et al.*[16] studied the sound-absorption predictions of perforated closed-cell metallic foams. They chose a microstructure-based model approach, and they compared the model with the experimental results. The porous media used in their study included DE pores created by perforating solids incorporating gas inclusions (closed porosity). They observed that these kinds of DE pores could have significant effects on the media acoustic behavior. The calculations showed that large pores increase the tortuosity; consequently, increasing the cellule diameter improves the normal sound absorption maximum peak value, and its frequency shifts toward lower frequencies. Furthermore, it showed that the local geometry parameters governing the pore/perforation relative position do not have significant effects on the sound-absorption behavior.

To model the acoustic behavior of this kind of porous material, it is, therefore, important to take into account the effect of the DE pores. This complex geometry is not taken into account in the classical equivalent fluid models.[2] Based on a simple approach, a new model is proposed to account for the presence of DE porosity in the material as along with the complexity of pore shapes. It includes two new parameters in addition to the five parameters (Biot porosity, tortuosity, static flow resistivity, viscous, and thermal characteristic lengths) of the classical Johnson-Champoux-Allard model. The new parameters are: the DE porosity, ϕ_{DE}, and an average length of the DE pores, l_{DE}. Comparison of the results provided by the modified model with experimental results seems to yield a better match. In order to validate the present model, a comparison between theoretical and experimental results was carried out on a "simplified sample" (a sample with well-controlled microstructural parameters) and on a porous metallic foam that is likely to incorporate dead end pores. Sections of the present article were presented at a conference.[17]

II. MODEL FOR DEAD-END POROSITY

A. Simple model at the microscopic scale

As mentioned in Sec. I, DE porosity is known in geophysics[5] and its effects have been observed on some porous materials in acoustics.[5–18] However, to our knowledge, no refined model of acoustic wave propagation in media with this micro-structural feature has been published.

Figure 2 also reveals the presence of narrow channels between the cavities. These very narrow constrictions are thought to be the cause of rotational flow with nonzero vorticity; however, this phenomenon is not studied here.

The presence of DE porosity in the studied materials is initially modeled at the microscopic level in terms of acoustic admittances, and then a homogenized version of a microscopic relationship between admittances is proposed. First, a circular duct of constant cross section, S, is considered, as shown in Fig. 4. This duct is acoustically characterized by its characteristic impedance, Z. The right end of the duct is connected to two auxiliary ducts, 1 and 2, of their respective characteristic impedances, Z_1 and Z_2, in the configuration of a Y-shaped junction. The two branches after the crossroad are also of constant section, S_1 and S_2, respectively.

This problem is a classical academic problem[19] and, assuming a left-to-right propagation from the principal branch to the secondary branches, the following relationship exists between admittances,

$$Y = Y_1 + Y_2, \tag{1}$$

where Y, Y_1, and Y_2 are, respectively, the acoustic admittances of the main branch and of branches 1 and 2, related to the characteristic impedance of each branch through the following relations,

$$Y = \frac{S}{Z}, \quad Y_1 = \frac{S_1}{Z_1}, \quad Y_2 = \frac{S_2}{Z_2}. \tag{2}$$

The characteristic impedances Z, Z_1, and Z_2 normalized by the sections are referred to as "acoustic impedances."[19]

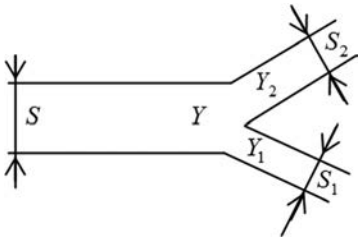

FIG. 4. Y-shaped junction between three branches in a porous medium.

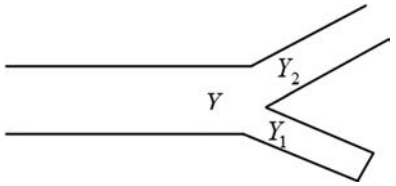

FIG. 5. Y-shaped junction in a porous medium with one branch closed.

It is now considered that one of the branches (branch 1, for example) is closed (see Fig. 5). The previous relation (1) remains valid with the difference that Y now represents a local admittance at the end of the main branch while Y_1 corresponds to the local admittance at the entrance of branch 1.

If branch 1 has a constant cross section and if the closing wall is rigid and perpendicular to the branch axis, the admittance, Y_1, is given by,

$$Y_1 = \frac{S_1}{-jZ_C \operatorname{cotan}(kl)}, \tag{3}$$

where Z_C is the characteristic impedance of air, k is the wavenumber, l is the length of branch 1, and j is the unit imaginary complex number (a time dependence in $\exp(j\omega t)$ has been chosen, with ω being the angular frequency).

B. Model at the macroscopic scale and average length of the dead ends

It is assumed that, at the frequencies considered, the wavelengths are much greater than the characteristic sizes of the microstructure. The behavior described at the microscopic scale can then be homogenized,

$$\bar{Y} = \bar{Y}_1 + \bar{Y}_2, \tag{4}$$

where $\bar{Y}$, $\bar{Y}_1$ and $\bar{Y}_2$ represent the averaged quantities associated with Y, Y_1, and Y_2, respectively, in a homogenization volume in the porous medium. In addition, it is assumed that in the studied materials, the cross sections of all branches are statistically uniform so that they do not play a role in Eq. (4).

This last equation can be easily interpreted. For a linear propagation, the acoustic behavior of a material containing DE pores is given by the sum of two contributions: $\bar{Y}_2$ associated with the fully open pores and $\bar{Y}_1$ associated with the partially open pores (DE pores). The volume proportion of the DE pores will be denoted as ϕ_{DE} (for $\phi_{Dead\ End}$) while the porosity of the fully opened pores will be denoted as ϕ_B (for ϕ_{Biot}). These two porosities are related to the total open porosity through the relation,

$$\phi = \phi_B + \phi_{DE}. \tag{5}$$

A pore can be considered "fully opened" if, when considering a slab of material at the laboratory scale, one can find a path connecting the front and the rear surface of the slab; the pore being connected to the exterior by both ends. A "partially opened" or "DE" pore would be one with only one end connected to either the front or the rear surface of the slab. It is important to make a distinction between the "opened porosity," ϕ, and the porosity of the "connected effective pores," ϕ_B (the former will always be greater than or equal to the latter). Among the open pores, some can be closed at one end.

The $\bar{Y}_2$ contribution is that of the pore that verifies the assumptions of the Johnson-Champoux-Allard model. It can be expressed as,

$$\bar{Y}_2 = \frac{1}{\bar{Z}_B}, \tag{6}$$

where $\bar{Z}_B$ is the characteristic impedance of the classical model, defined only for fully opened pores of porosity, ϕ_B.

From Eq. (3), one can define for $\bar{Y}_1$ an average value, integrated over a homogenization volume, V_{DE}, of dead end pores

$$\bar{Y}_1 = \frac{j}{Z_C} \frac{\iiint_{V_{DE}} \tan(kl) dV}{\iiint_{V_{DE}} dV}. \tag{7}$$

If the additional assumption, $kl \ll 1$ is made, Eq. (7) becomes, to the first order

$$\bar{Y}_1 \approx \frac{jk}{Z_C} \frac{\iiint_{V_{DE}} l dV}{\iiint_{V_{DE}} dV}. \tag{8}$$

This assumption is valid for DE pores that are much shorter than any acoustic wavelength. This allows us to define an average length of the DE pores by,

$$l_{DE} = \frac{\iiint_{V_{DE}} l dV}{\iiint_{V_{DE}} dV}. \tag{9}$$

The admittance (8) is finally expressed as,

$$\bar{Y}_1 \approx \frac{jkl_{DE}}{Z_C}. \tag{10}$$

1. Remarks

(a) The homogenization process is implied in Eq. (4), which is proposed without demonstration. By writing Eq. (4), we assume that the effects of each dead end can be added up (superposed), resulting in a global contribution to the admittance if there are enough dead ends per unit volume of the homogenized porous aggregate. It is believed that the superposition of the effects of the dead ends is valid since we consider the wave propagation in the linear regime. The validity of Eq. (4) will be studied in future work.

(b) To illustrate this approach, an example of a material with simple geometries is proposed (see Fig. 6); in this material, it is clear that $l_{DE} = d$. With definition (9), this result is easily retrieved,

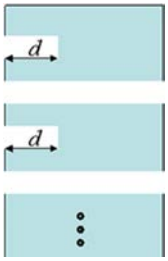

FIG. 6. (Color online) Example of a material with simple geometries, used to illustrate the l_{DE} formulation.

$$l_{DE}=\frac{\iiint_{V_{DE}} l dV}{\iiint_{V_{DE}} dV}=\frac{Vd+Vd+\cdots+Vd}{V+V+\cdots+V}=\frac{nVd}{nV}=d. \quad (11)$$

(c) In the framework of the effective fluid approach of Biot,[20,21] the following length could be defined (instead of that of Eq. (9)):

$$l_{DE}^{eff}=\frac{\iiint_{V} l dV}{\iiint_{V} dV}, \quad (12)$$

where V is a homogenization volume of the bulk material involving the porous aggregate (solid + fluid).

C. Accounting for dissipations in dead-end pores

The previous equations for $\bar{Y}_1$were established from a simple modeling of a DE pore at the microscopic scale as a closed duct. To account for viscous and thermal dissipations in the DE pores at the macroscopic scale, it suffices to replace Z_C and k by those provided by the Johnson-Champoux-Allard model applied to the volume fraction of DE pores,

$$Z_C \rightarrow \bar{Z}_{DE} \quad \text{and} \quad k \rightarrow \bar{k}_{DE}, \quad (13a)$$

while, when applied to the volume fraction of the kinematic pores (the Biot porosity), one should use

$$Z_C \rightarrow \bar{Z}_B \quad \text{and} \quad k \rightarrow \bar{k}_B. \quad (13b)$$

Other remarks can be made about the model:

(a) Equation (4) indicates that the sole contribution, $\bar{Y}_2$, would correspond to a simple porosity correction. The additional contribution, $\bar{Y}_1$, accounts for the standing wave fields created in the DE pores.
(b) The principle of the model of acoustic wave propagation in porous materials including DE pores can be summarized with the schematic shown in Fig. 7.
(c) The assumptions of the proposed model are the same as those of the classical model. One additional assumption has been added on the length of the DE pores.
(d) This model does not account for the presence of narrow constrictions in the material that are thought to be responsible for local flows with vorticity, even at low average flow velocity.

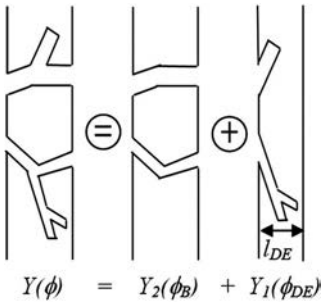

FIG. 7. Principle of the model incorporating DE pores.

D. Recall of the Johnson-Champoux-Allard model

This section recalls the main results of the Johnson-Champoux-Allard model.[2,4,22] This model is based on five macroscopic parameters: porosity, ϕ, static airflow resistivity, σ, tortuosity, α_∞, viscous characteristic length, Λ, and thermal characteristic length, Λ'. In the rigid-frame approximation, the solid matrix (skeleton) is considered to be much heavier and more rigid than the saturating air. As pointed out by Panneton,[23] several approaches (effective or equivalent approaches) can be used to describe the complex density and bulk modulus of the slab. The approach used here consists of considering the slab of porous material in the rigid frame approximation as a slab of equivalent fluid with the following density, $\rho_{eq}(\omega)$, and bulk modulus, $K_{eq}(\omega)$:

$$\rho_{eq}(\omega)=\frac{\alpha_\infty \rho_f}{\phi}\left(1-j\frac{\omega_c}{\omega}F(\omega)\right), \quad (14)$$

$$K_{eq}(\omega)=\frac{1}{\phi}\frac{\gamma P_0}{\gamma-(\gamma-1)\quad 1-j\dfrac{8\eta}{B^2\omega\Lambda'^2\rho_f}G(B^2\omega)}^{-1}, \quad (15)$$

with

$$\omega_c=\frac{\sigma\phi}{\rho_f\alpha_\infty}, \quad (16)$$

where η is the dynamic viscosity, B^2 is the Prandtl number, γ is the constant pressure and volume specific heat ratio (sometimes referred to as the adiabatic constant), and P_0 is the atmospheric static pressure. The parameter, ω_c, is Biot's cutoff angular frequency separating Biot's high and low frequency ranges.

The functions, $F(\omega)$ and $G(B^2\omega)$, are the correction functions introduced, respectively, by Johnson *et al.*[22] and by Champoux and Allard.[4] They are given by,

$$F(\omega)=\sqrt{1+j\frac{4\eta\rho_f\alpha_\infty^2}{\phi^2\sigma^2\Lambda^2}\omega}, \quad (17)$$

and

$$G(B^2\omega)=\sqrt{1+j\frac{\rho_f\Lambda'^2B^2\omega}{16\eta}}. \quad (18)$$

All of the necessary parameters for the acoustic characterization of porous layers are easily deduced with the help of $\rho_{eq}(\omega)$ and of $K_{eq}(\omega)$. In particular, the characteristic impedance and wave number of are given by,

$$\bar{Z}(\omega) = \sqrt{\rho_{eq}(\omega)K_{eq}(\omega)} \quad \text{and} \quad \bar{k}(\omega) = \omega\sqrt{\frac{\rho_{eq}(\omega)}{K_{eq}(\omega)}}. \quad (19)$$

It is worth mentioning that these expressions (ρ_{eq}, K_{eq}, $\bar{Z}$, and $\bar{k}$) can be applied to the open pores and to the DE pores with special attention on the choice of the macroscopic properties (notably $\phi = \phi_{DE}$ for the DE domain, and $\phi = \phi_B$ for the Biot domain).

1. Remarks

The DE geometry complexities are taken into account via its DE equivalent parameters (Z, k). Consequently, the present model can account for different kinds of DE pores:

(a) Pores without constriction (straight pores).
(b) Ink-bottle pores or Helmholtz resonators.
(c) Complex pores with cells and constrictions.

E. Correction of the Johnson-Champoux-Allard model to include dead-end pores

The correction that includes the effect of DE pores is implemented through the use of Eq. (4)–(6) and (10) in order to calculate $\bar{Y}(\phi)$. Following Fig. 7, the Johnson-Champoux-Allard model is first applied on a material of porosity, ϕ_B, to determine $\bar{Y}_2(\phi_B)$ and then a second time in order to determine$\bar{Y}_1(\phi_{DE})$. In the second application of the model, a slab of thickness, l_{DE}, and of porosity, ϕ_{DE}, must be considered. The acoustical properties of the material containing DE pores are finally deduced from $\bar{Y}(\phi)$, given by Eq. (4).

F. Transfer matrix method

In acoustics, the transfer matrix method is a powerful method to optimize and predict sound absorption and sound transmission of single layer and multilayer sound absorbing materials.[2] In the following text, transfer matrices will be developed for the studied rigid-frame porous aggregate containing DE porosity for non-symmetric and symmetric configurations.

1. Non-symmetric configuration

A vertically periodic unit cell of a non-symmetric porous medium with DE porosity is shown in Fig. 8. Here, the porous medium separates two fluid domains. The cell is divided into two porous elements in parallel. The first element (element DE) is the one representing the DE porosity (non-symmetric element). The second one is the BIOT element containing pores that are opened on both ends only (symmetric element), with the whole being non-symmetric. Each element has equivalent macroscopic properties averaged over a representative homogeneous volume. To link acoustic pressures and velocities on both faces of the material, a transfer matrix relation can be developed.

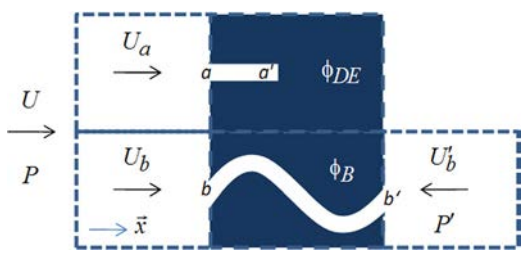

FIG. 8. (Color online) Principle of the model including the non-symmetric DE element.

For the DE element, the transfer matrix relation is given by,

$$\begin{Bmatrix} P_a \\ U_a \end{Bmatrix} = [T]^{DE} \begin{Bmatrix} P'_a \\ -U'_a \end{Bmatrix}, \quad (20)$$

with

$$[T]^{DE} = \begin{bmatrix} t_{11}^{de} & t_{12}^{de} \\ t_{21}^{de} & t_{22}^{de} \end{bmatrix} = \begin{bmatrix} \cos(\bar{k}_{DE} l_{DE}) & j\bar{Z}_{DE} \sin(\bar{k}_{DE} l_{DE}) \\ \frac{j}{\bar{Z}_{DE}} \sin(\bar{k}_{DE} l_{DE}) & \cos(\bar{k}_{DE} l_{DE}) \end{bmatrix}, \quad (21)$$

where the prime symbol is assigned to an output port variable and the averaged length and equivalent fluid properties are obtained from Eqs. (9) and (19), respectively. Here, the minus sign is added to take into account the fact that velocity is defined following the inward normal to the element. Since the elements are in parallel, it is preferred to work with admittances as presented in Sec. II A. Consequently, Eq. (20) can be rewritten in terms of an admittance matrix as

$$\begin{Bmatrix} U_a \\ U'_a \end{Bmatrix} = [Y]^{DE} \begin{Bmatrix} P_a \\ P'_a \end{Bmatrix}, \quad (22)$$

with

$$[Y]^{DE} = \begin{bmatrix} y_{11}^{de} & y_{12}^{de} \\ y_{21}^{de} & y_{22}^{de} \end{bmatrix} = \begin{bmatrix} \frac{t_{22}^{de}}{t_{12}^{de}} & -\frac{1}{t_{12}^{de}} \\ -\frac{1}{t_{12}^{de}} & \frac{t_{11}^{de}}{t_{12}^{de}} \end{bmatrix}. \quad (23)$$

Since, at the end of the DE pore, the velocity vanishes ($U'_a = 0$), the previous transfer matrix yields,

$$P'_a = -\frac{y_{21}^{de}}{y_{22}^{de}} P_a. \quad (24)$$

For the BIOT element, the transfer matrix relation is given by

$$\begin{Bmatrix} P_b \\ U_b \end{Bmatrix} = [T]^{B} \begin{Bmatrix} P'_b \\ -U'_b \end{Bmatrix}, \quad (25)$$

with

$$[T]^{B} = \begin{bmatrix} t_{11}^{b} & t_{12}^{b} \\ t_{21}^{b} & t_{22}^{b} \end{bmatrix} = \begin{bmatrix} \cos(\bar{k}_B l) & j\bar{Z}_B \sin(\bar{k}_B l) \\ \frac{j}{\bar{Z}_B} \sin(\bar{k}_B l) & \cos(\bar{k}_B l) \end{bmatrix}, \quad (26)$$

where the equivalent fluid properties are, respectively, obtained from Eqs. (9) and (19) and correspond to the porous

material without DE pores. The corresponding admittance matrix is given by

$$\begin{Bmatrix} U_b \\ U'_b \end{Bmatrix} = [Y]^B \begin{Bmatrix} P_b \\ P'_b \end{Bmatrix}, \tag{27}$$

with

$$[Y]^B = \begin{bmatrix} y^b_{11} & y^b_{12} \\ y^b_{21} & y^b_{22} \end{bmatrix} = \begin{bmatrix} \frac{t^b_{22}}{t^b_{12}} & -\frac{1}{t^b_{12}} \\ -\frac{1}{t^b_{12}} & \frac{t^b_{11}}{t^b_{12}} \end{bmatrix}. \tag{28}$$

Invoking continuity of pressure ($P = P_a = P_b$) and continuity of flow rate ($SU = S(U_a + U_b)$) at the air-element interfaces, Eqs. (22), (24), and (28) yield,

$$\begin{cases} U = \left(y^b_{11} + y^{de}_{11} - \frac{\left(y^{de}_{12}\right)^2}{y^{de}_{22}} \right) P + y^b_{12} P'_b \\ U'_b = y^b_{12} P + y^b_{22} P'_b \end{cases}. \tag{29}$$

Here, it is worth mentioning that U_a and U_b are the macroscopic fluid velocity in the fluid domain in front of each element, respectively. They are related to the velocity in the pores by $U_a = \phi_{DE} u_a$ and $U_b = \phi_B u_b$. Consequently, this yields, at the macroscopic scale, the continuity of velocity: $U = \phi_{DE} u_a + \phi_B u_b$.

By solving Eq. (29) for P and U, the non-symmetric matrix system can be written as,

$$\begin{Bmatrix} P \\ U \end{Bmatrix} = [T]^{NS} \begin{Bmatrix} P'_b \\ -U'_b \end{Bmatrix}, \tag{30}$$

with

$$[T]^{NS} = \frac{1}{y^b_{12}} \begin{bmatrix} -y^b_{22} & -1 \\ \left(y^b_{12}\right)^2 - y^b_{22}\left(y^b_{11} + y^{de}_{11} - \frac{\left(y^{de}_{12}\right)^2}{y^{de}_{22}} \right) & -\left(y^b_{11} + y^{de}_{11} - \frac{\left(y^{de}_{12}\right)^2}{y^{de}_{22}} \right) \end{bmatrix}. \tag{31}$$

Matrix $[T]^{NS}$ is the transfer matrix of the two elements in parallel. The index, *NS*, is chosen for the *non-symmetric* DE element. This system preserves the reciprocity principle since $\det[T]^{NS} = 1$; however, it is not of a symmetric nature (i.e., $t^{ns}_{11} \neq t^{ns}_{22}$). The validation of this approach will be discussed in the experimental part of the present study.

2. Symmetric configuration

Now, the element is assumed symmetric, which means that DE pores are seen on both faces of the equivalent element. This type of element is shown in Fig. 9. For this case, the previous approach is used to establish the transfer matrix of the porous aggregate with DE porosity.

At first, it is important that the BIOT element be divided in two along the thickness. Consequently, the sample has a thickness that is half the total thickness (i.e., $l \rightarrow l/2$) and the middle is located at point b'. It is assumed that the DE and BIOT elements have homogeneous properties along the thickness. In this case, the porosities, ϕ_{DE} and ϕ_B, are the same for the first and second halves. Note that since the DE porosity is seen equivalently by incident waves on both faces of the sample, the DE pore thickness is the same for the first and second halves and is given by the averaged length, l_{DE}. Even if, in Fig. 9, the DE porosity seems virtually doubled, the porosity stays as ϕ_{DE}.

With the previous description, the transfer matrix of the first half is computed as was done in the previous section. The only change is to use $l/2$ instead of l. In this case, the transfer matrix relation of the first half is written as,

$$\begin{Bmatrix} P \\ U \end{Bmatrix} = [T]_A \begin{Bmatrix} P'_b \\ -U'_b \end{Bmatrix}, \tag{32}$$

where $[T]_A = [T(l/2)]^{NS}$ is the transfer matrix of the first half of the porous aggregate with the DE porosity on the front surface.

For the second half, a similar development is performed. For the DE pore on the right, the following relations are developed:

$$\begin{Bmatrix} P'''_a \\ U'''_a \end{Bmatrix} = \begin{bmatrix} t^{de}_{11} & t^{de}_{12} \\ t^{de}_{21} & t^{de}_{22} \end{bmatrix} \begin{Bmatrix} P''_a \\ -U''_a \end{Bmatrix}, \tag{33}$$

and

$$\begin{Bmatrix} U'''_a \\ U''_a \end{Bmatrix} = \begin{bmatrix} y^{de}_{11} & y^{de}_{12} \\ y^{de}_{21} & y^{de}_{22} \end{bmatrix} \begin{Bmatrix} P'''_a \\ P''_a \end{Bmatrix}. \tag{34}$$

With the boundary condition, $U'''_a = 0$, the previous equation yields

$$P'''_a = -\frac{y^{de}_{21}}{y^{de}_{22}} P''_a. \tag{35}$$

For the second half of the BIOT element (i.e., from b' to b''), the following relations are developed:

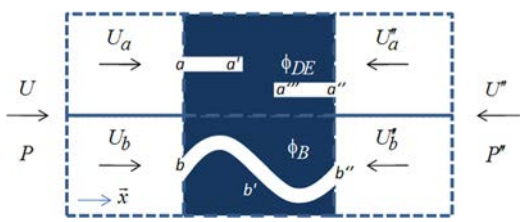

FIG. 9. (Color online) Principle of the model including the symmetric DE element.

$$\begin{Bmatrix} P'_b \\ U'_b \end{Bmatrix} = \begin{bmatrix} t^b_{11} & t^b_{12} \\ t^b_{21} & t^b_{22} \end{bmatrix} \begin{Bmatrix} P''_b \\ -U''_b \end{Bmatrix}, \tag{36}$$

and

$$\begin{Bmatrix} U'_b \\ U''_b \end{Bmatrix} = \begin{bmatrix} y^b_{11} & y^b_{12} \\ y^b_{21} & y^b_{22} \end{bmatrix} \begin{Bmatrix} P'_b \\ P''_b \end{Bmatrix}. \tag{37}$$

Invoking the continuity of pressure and continuity of flow rate at the air-element interfaces, and solving for P'_b and U'_b, the transfer matrix relation of the second half is written as,

$$\begin{Bmatrix} P'_b \\ U'_b \end{Bmatrix} = [T]_B \begin{Bmatrix} P'' \\ -U'' \end{Bmatrix}, \tag{38}$$

where $[T]_B$ is the transfer matrix of the second half of the porous aggregate with the DE porosity on the rear surface. It is given by

$$[T]_B = \frac{1}{y^b_{12}} \begin{bmatrix} -\left(y^b_{22} + y^{de}_{22} - \frac{\left(y^{de}_{12}\right)^2}{y^{de}_{11}}\right) & -1 \\ \left(y^b_{12}\right)^2 - y^b_{11}\left(y^b_{22} + y^{de}_{22} - \frac{\left(y^{de}_{12}\right)^2}{y^{de}_{11}}\right) & -y^b_{11} \end{bmatrix}. \tag{39}$$

To form the global transfer matrix of the whole symmetrical porous aggregate with the DE porosity, the chain rule on transfer matrix multiplication is used. This gives,

$$\begin{Bmatrix} P \\ U \end{Bmatrix} = [T]^S \begin{Bmatrix} P'' \\ -U'' \end{Bmatrix}, \tag{40}$$

with

$$[T]^S = [T]_A [T]_B. \tag{41}$$

3. Remarks

(a) This transfer matrix has the following properties: reciprocity (i.e., $\det[T]^S = 1$), symmetry of the material (i.e., $t^s_{11} = t^s_{22}$), and compatibility with other classical transfer matrices.[2]
(b) This approach can be adapted to heterogeneous DE materials with different DE parameters on each half.
(c) If $[T]_A$ is computed with thickness, l, instead of $l/2$, then the non-symmetric matrix $[T]^{NS}$ of Sec. II F 1 is found. If $[T]_B$ is computed with thickness, l, instead of $l/2$, then a similar non-symmetric model is found; however, this time the DE pores are localized on the other side. In conclusion, the symmetric transfer matrix model encompasses the non-symmetric model and is, therefore, more general.

G. Acoustical indicators

1. Sound transmission loss

From the transfer matrix approach, it is easy to study the sound transmission of a porous material with DE porosity. The global transfer matrix of a porous media with DE porosity is, $[T]^{mat}$. This matrix must be adapted to the particular case under study. If a non-symmetric configuration with the DE pores on the front face is considered, then $[T]^{mat} = [T]^{NS} = [T(l)]_A$. If the DE pores are on the rear face, then $[T]^{mat} = [T(l)]_B$. If a symmetric configuration is considered, then $[T]^{mat} = [T]^S$. From the appropriate transfer matrix, the sound transmission coefficient and the transmission loss in normal incidence are given by

$$|\tau| = \left| \frac{2}{t^{mat}_{11} + t^{mat}_{22} + t^{mat}_{12}/Z_0 + t^{mat}_{21} Z_0} \right|, \tag{42}$$

and

$$TL = -20 \log_{10}(|\tau|), \tag{43}$$

where Z_0 is the characteristic impedance of the air.

2. Sound absorption coefficient

To obtain the sound absorption coefficient from the transfer matrix method, one first needs to define the backing condition and use the appropriate system transfer matrix, $[T]^{syst}$. If the porous material with DE porosity is backed by a rigid wall, $[T]^{syst} = [T]^{mat}$. If the porous material with DE porosity is backed by an air cavity and a rigid wall, $[T]^{syst} = [T]^{mat}[T]^{cav}$, with

$$[T]^{cav} = \begin{bmatrix} \cos(k_0 l_{cav}) & jZ_0 \sin(k_0 l_{cav}) \\ \frac{j}{Z_0}\sin(k_0 l_{cav}) & \cos(k_0 l_{cav}) \end{bmatrix}, \tag{44}$$

where k_0 is the wave number of air, and l_{cav} is the depth of the cavity. Then, from the appropriate system transfer matrix, the normal incidence surface impedance of the studied configuration is given by,

$$Z_S = \frac{t^{syst}_{11}}{t^{syst}_{21}}, \tag{45}$$

and the normal sound absorption coefficient is given by,

$$\alpha_N = 1 - \left| \frac{Z_S - Z_0}{Z_S + Z_0} \right|^2. \tag{46}$$

III. EXPERIMENTAL RESULTS

A. Simplified sample

To confirm the validity of the exposed model, a simplified non-symmetric sample with well-controlled parameters was tested. The sample consists of a circular column of

FIG. 10. (Color online) Photo of the simplified non-symmetric sample. Face A (left) includes all pores. Face B (right) only includes effective pores (without DE pores).

Teflon which is perforated with regular cylindrical perforations (see Fig. 10). Some perforations are complete (they represent the kinematic porosity), while others are incomplete or semi-closed (they represent the DE porosity). The open ends are only visible on one face of the sample (face A). The depth of the semi-closed holes is $l_{DE} = 25$ mm, the sample thickness is $l = 30$ mm, its diameter is 44.4 mm, the perforation diameter is $d = 2$ mm, and the minimum perforation constriction is $d_{min} = 1.8$ mm (error due to the perforation process). The porosities are $\phi_B = 14\%$, $\phi_{DE} = 13.5\%$. Table I summarizes the DE parameters of the tested sample.

For this kind of simple material, the Johnson-Champoux-Allard (JCA) parameters are easily defined for both the Biot and DE domains. The viscous and thermal lengths, the tortuosity and the resistivity are given, respectively, by JCA's parameters for cylindrical pores:[2] $\Lambda' = d/2$, $\Lambda = d_{min}/2$, $\alpha_\infty = 1$, and $\sigma = 32\eta/\phi d^2$, where η is the dynamic viscosity of air and ϕ is the open porosity (use ϕ_B for the Biot domain; use ϕ_{DE} for the DE domain). Since the sample thickness is large compared to the perforation diameter, the sound radiation of the perforation openings in open air is not considered here.

A three-microphone impedance tube is used to measure the normal sound absorption coefficient and sound transmission loss of the sample coupled to an air cavity and a rigid termination. The frequency range between 200 Hz and 4200 Hz was chosen to ensure that only plane waves exist in the tube (the tube diameter is 44.45 mm; the cut-off frequency is 4400 Hz). The two microphones upstream of the sample are used to measure the sound absorption by the standard impedance tube measurement technique.[24] Since the simplified sample is non-symmetric, the sound absorption coefficient of each face will be measured. A third microphone, localized on the hard wall backing (behind the backing cavity), measures the transfer matrix and deduces the transmission loss by way of the "three-microphones and two-cavity method."[25] For the transmission loss measurement, the choice of surface exposition of the non-symmetrical material is not important since the reciprocity principle applies on the transmission. The sound pressure excitation is random noise in the linear regime. The majority of repeatability errors occur from the way the sample is positioned in the tube: special attention was therefore paid to this positioning. However, since this error is low for these measurements, their associated error bars are not presented as graphs.

TABLE I. Dead-end parameters of the non-symmetric simplified sample.

Total porosity (%)	ϕ_B (%)	ϕ_{DE} (%)	l_{DE} (mm)
27.5	14	13.5	25

The results, which are presented in Figs. 11 and 12, correspond to the configuration where face A (showing the DE pores) is on the source side. Figure 11(a) shows the comparison between the experimental results and the models' predictions (present model and JCA model) of the absorption coefficient of the simplified non-symmetric sample coupled to a 20-mm air cavity gap and a rigid wall. The present model with the non-symmetric transfer matrix given by $[T(l)]_A$ is used. The first absorption peak (around 750 Hz) represents the air cavity effect, and the second peak (around 3300 Hz) represents the semi-closed hole effect (i.e., DE porosity effect) on the excitation side. Compared to the JCA model (where only kinematic porosity is taken into account), the present model improves the comparison with experiments. In fact, the present model precisely predicts the frequency position of the two peaks, although the absorption peak values are slightly different. The comparison between the experiments and predictions for a different air cavity gap ($l_{cav} = 50$ mm) is presented in Fig. 11(b). Around 3300 Hz, the air cavity effect and the DE porosity effect are coupled

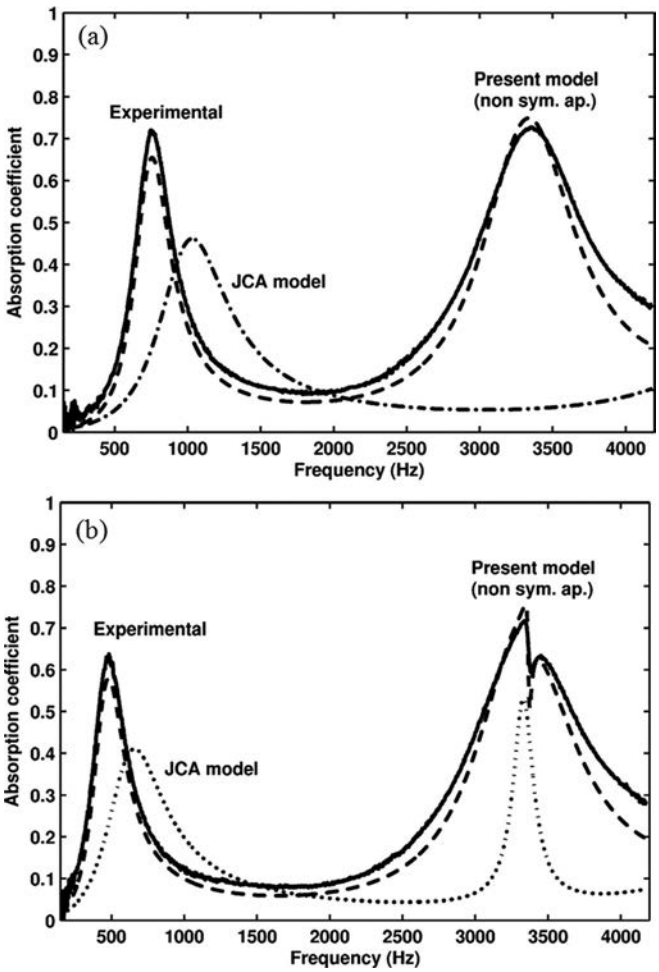

FIG. 11. Comparison between the experimental results and the models' predictions of the absorption coefficient of the simplified non-symmetric sample coupled to an air cavity and a rigid wall. Face A (showing DE pores) is on the source side. (a) 20-mm thick air cavity. (b) 50-mm thick air cavity.

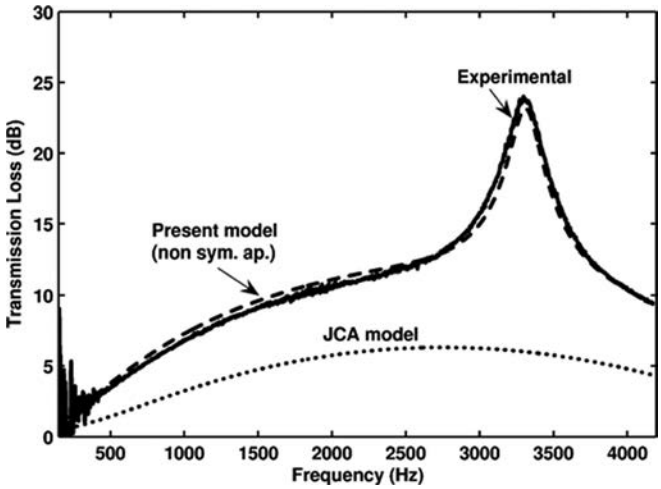

FIG. 12. Comparison between the experimental results and the models' predictions of the transmission loss of the simplified non-symmetric sample. Face A (showing DE pores) is on the source side.

on the absorption coefficient: note that the present model accounts for this coupling effect.

Figure 12 presents the comparison between the experimental results and the models' predictions of the transmission loss of the simplified non-symmetric sample. Here, the presence of the DE pores significantly modifies the transmission loss: a large peak of transmission loss appears around 3300 Hz. The frequency position of this transmission loss peak is quite dependent on the value of l_{DE}. Good agreement is obtained between the present model and the experimental results.

Figures 13 and 14 present the sound absorption and transmission loss of the same simplified non-symmetric sample, however, this time the sample is inverted in the tube. Contrary to the previous results, the DE pores (face A) are now facing the backing air cavity and rigid wall. Hence, the non-symmetric matrix given by $[T(l)]_B$ is used. Figure 13 presents the comparison between the experiments and the predictions for the absorption coefficient of the simplified non-symmetric sample coupled to two different air cavity gaps: $l_{cav} = 20$ mm and $l_{cav} = 50$ mm. The experimental and simulated results are logically quite different compare to the preceding part, particularly concerning the absorption peak caused by the DE pores. For $l_{cav} = 20$ mm, this peak almost disappears. Only a very small peak emerges around 3300 Hz. For $l_{cav} = 50$ mm, three absorption peaks can be observed: the first two correspond to the Biot pore coupled with the air cavity effect, while the third peak corresponds to the DE pore coupled with the air cavity effect. For the sound absorption coefficient, the comparison between the experimental results and the present model's predictions is satisfactory.

In Fig. 14, the simulated transmission loss in the inverted configuration is logically equivalent to the one previously obtained in Fig. 12 due to the reciprocity of the transfer matrix. Similarly, the experimental results are not very different from those presented in Fig. 12. The slight differences may be attributed to experimental errors and to the positioning in the tube when the sample was inverted.

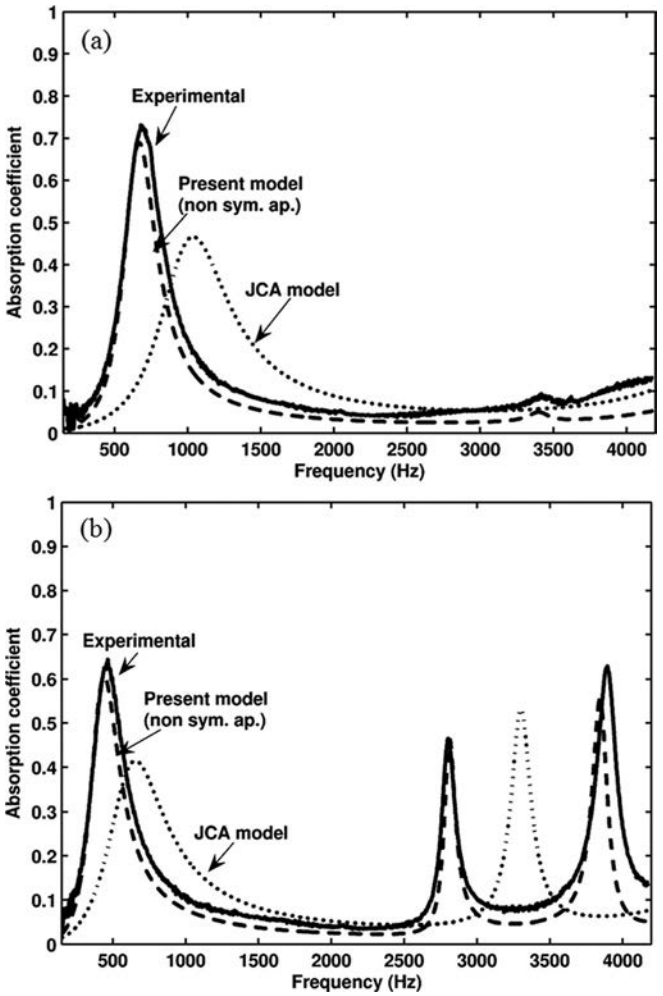

FIG. 13. Comparison between the experimental results and the models' predictions of the absorption coefficient of the simplified non-symmetric sample coupled to an air cavity and a rigid wall. Face A (showing DE pores) is on the backing cavity side. (a) 20-mm thick air cavity. (b) 50-mm thick air cavity.

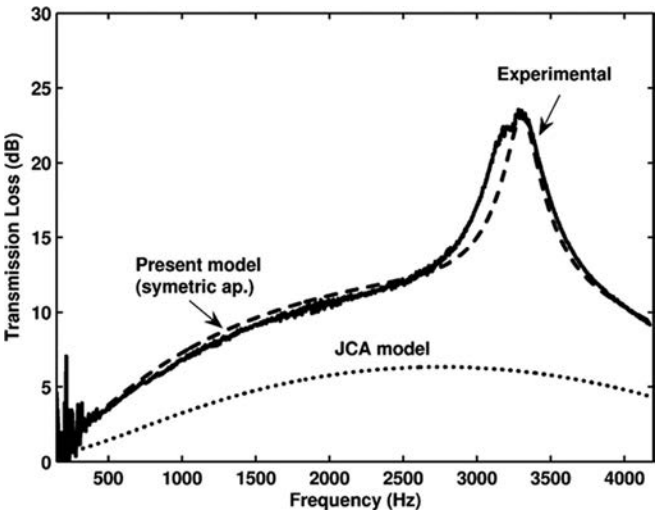

FIG. 14. Comparison between the experimental results and the models' predictions of the transmission loss of the simplified non-symmetric sample. Face A (showing DE pores) is on the source side.

In this section, a simplified sample was presented to validate the present model and to show the importance of accounting for the DE porosity. The comparisons between the predictions of the present model and the experimental results are in good agreement for both the sound absorption coefficient and the sound transmission loss. Similar results were also obtained for a series of other simplified nonsymmetrical samples with different parameters. For the sake of simplicity, these results were not reported here. The following section will test the present model with a more complex and more realistic material than the simplified nonsymmetrical sample.

B. Aluminum foam sample

In this study, a number of different aluminum foams were tested and one has been selected for presentation in this article (see Fig. 15). The base material used was AS7 G aluminum. The Johnson-Champoux-Allard (JCA) parameters of the aluminum foam have first been measured. The static airflow resistivity, σ, and global porosity, ϕ, have been measured by a resistivity meter and a weight differential approach, repectively.[26,27] To characterize the tortuosity, α_∞, and characteristic lengths, Λ and Λ', the ultrasound method has been used.[28–31] This method allows for the measurement of the equivalent length,

$$L_{eq} = \left(\frac{1}{\Lambda} + \frac{\gamma - 1}{B\Lambda'}\right)^{-1}, \tag{47}$$

where γ is the adiabatic constant of gas and B^2 is the Prandtl number.

The L_{eq} values were found to be very weak, suggesting that the constrictions between two cells are very narrow. This can be seen on the microstructure pictures (Fig. 2), which also allows for the observation of the pore size. The ratio between Λ' and Λ was difficult to find; the typical ratio for classical material is generally between 2 and 4. Therefore, image analysis was used on several images to estimate Λ'/Λ: microscope pictures of transversal and longitudinal cross-sections of a material sample were taken with different light incidences, in order to improve the contrast of the picture and to clearly differentiate the surface open cells with the solid surface, and to differentiate the cell interstices with cells. Following this procedure, the mean pore size of the foam (d_{cell}) and the size of the interstices (d_{hole}) were obtained. In a first approximation, the ratio, Λ'/Λ, was identified by the ratio, d_{cell}/d_{hole}.

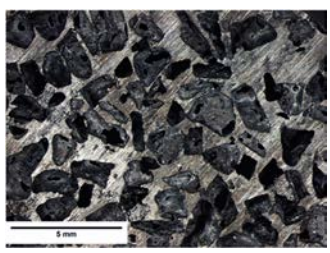

FIG. 15. (Color online) Photo of the surface of the tested aluminum foam.

TABLE II. Johnson-Champoux-Allard (JCA) parameters of the aluminum foam sample.

JCA parameters	Λ (μm)	Λ' (μm)	α_∞	σ (Pa s/m^2)	ϕ (%)
Mean value	101	352	2.25	19 713	64.5
Standard deviation	4	14	0.05	300	3

These experimental methods to define the JCA parameters introduce significant errors when applied to metallic foams; therefore, for each JCA parameter it is important to define a mean value, $\bar{x}$, and a standard deviation, $\sigma_{st.dev.}$, such that $x = \bar{x} \pm \sigma_{st.dev.}$. These errors were then included in the models (JCA and present models). In the figures, the models' predictions are represented with their error bars. The JCA acoustic parameters (mean value and standard deviation) are summarized in Table II. As will be shown, the errors on the JCA parameters introduce notable errors on the predictions of the transmission loss and sound absorption coefficient, which are more significant than those obtained with impedance tube measurements. To facilitate the readability of the results, only the error bars on the predictions are presented in the figures.

To take into account the DE porosity effect, the DE parameters (l_{DE} and ϕ_{DE}) had to be determined. For l_{DE}, a multiple of the statistical pore size was chosen: $l_{DE} = n\, d_{cell}$. To determine n and ϕ_{DE}, a fitting approach on the experimental results was used. Since it is very difficult to precisely define l_{DE} and ϕ_{DE} for these kinds of complex foams, work is in progress to estimate them; notably, from micro-tomography, acoustics low frequency methods, and ultrasound methods. The DE parameters used (mean value and standard deviation) are summarized in Table III. For the usual porous materials (without dead end), no simple link between microscopic geometry and macroscopic parameters exists except for simple geometries (cylindrical pores). Similarly, in our case, for simple cylindrical pores without constriction, the DE porosity would simply be that of the DE and the l_{DE} would be its length. For pores with more complicated shapes (ink bottle pores or pores with constrictions…) there is no straightforward interpretation of the microscopic/macroscopic link. The macroscopic characterization of these two DE parameters has been currently studied (for example, by ultrasonic techniques).

For this kind of material, it is preferable to use the symmetric transfer matrix, $[T]^S$, for predicting its acoustical indicators. In fact, due to the random nature of the fabrication process, the DE pores are dispersed throughout the material in a homogeneous manner.

TABLE III. Dead-end parameters of the aluminum foam sample (fitting and experimental approaches).

Total porosity (%)	ϕ_B (%)	ϕ_{DE} (%)	l_{DE} (mm)
64.5 ± 3	≈ 55	≈ 7.5	$\approx 7 d_{cell}$

1. Remark

At this stage of the research, we have chosen to use the same JCA parameters, measured on the global aluminum foams (see preceding text), for both the DE element (Λ_{DE}, Λ'_{DE}, $\alpha_{\infty DE}$, and σ_{DE}) and the Biot kinematic element (Λ_B, Λ_B, $\alpha_{\infty B}$, and σ_B). The choice of these parameters will have to be studied more precisely in the future.

As in the previous section, the impedance tube with the two-microphone technique is used to measure the sound absorption and the three-microphone technique is used to measure the sound transmission loss.

Figure 16 presents the comparison between the experimental results and the models' predictions ($[T]^S$ symmetric approach and JCA model) of the absorption coefficient of the studied aluminum foam sample coupled to: (a) a rigid wall ($l_{cav} = 1$ mm), and (b) a 50-mm air cavity backed by a rigid wall. One can note that the present approach and JCA model yield comparable results in terms of sound absorption and compare well with experiments. However, a slight shift toward low frequencies is observed with the present symmetric approach. This yields a better prediction of the absorption peaks. This seems to show that the present approach adds the necessary degree-of-freedom to capture the physics of the DE pores in the material, which are not captured with the JCA model.

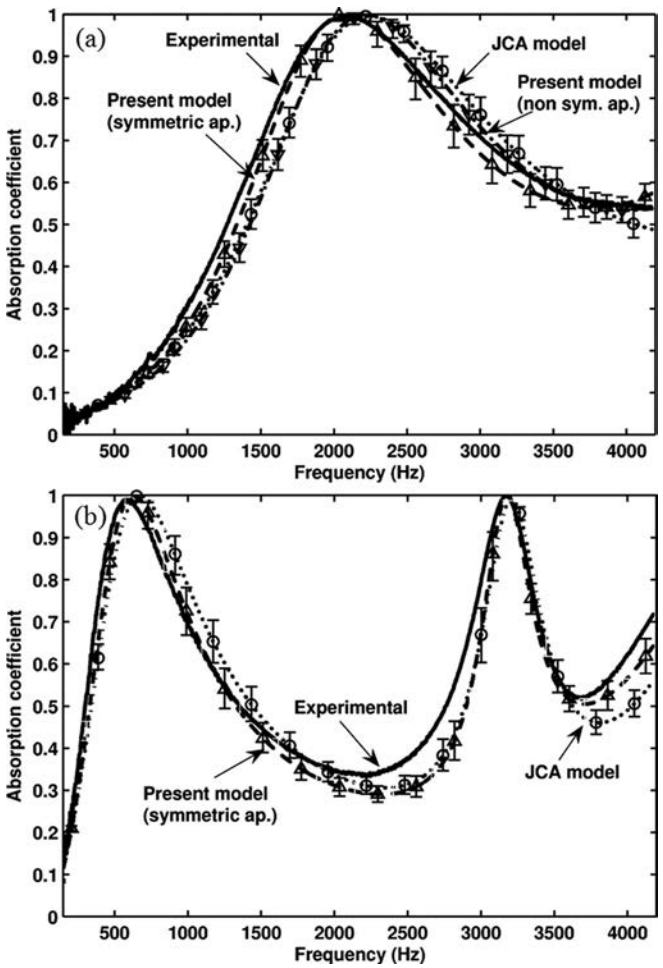

FIG. 16. Comparison between the experimental results and the models' predictions of the absorption coefficient of the aluminum foam sample. (a) Hard wall backing ($l_{cav} < 1$ mm). (b) Air cavity backing ($l_{cav} = 50$ mm) on hard wall.

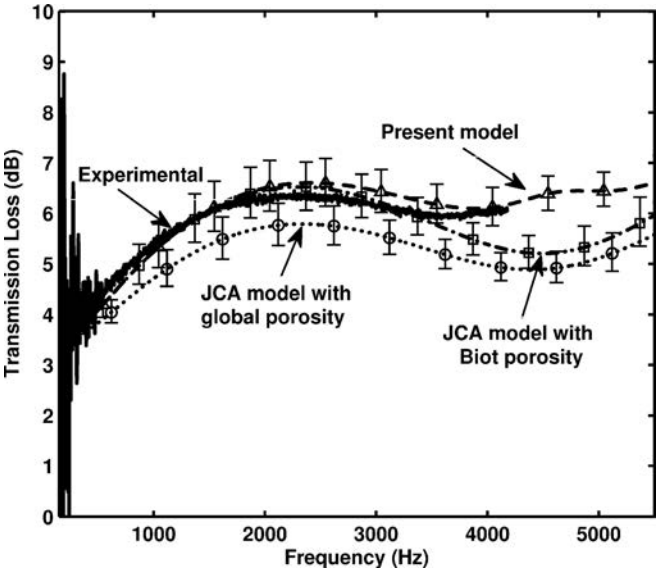

FIG. 17. Comparison between the experimental results and the models' predictions of the transmission loss of the aluminum foam sample. The frequencies bandwidths are 125 and 4200 Hz for the experimental results and 125 and 5500 Hz for the model results.

Figure 17 presents the comparison between the experimental results and the models' predictions on the transmission loss of the aluminum foam sample. The comparison between the present model and the experimental results is encouraging. Here, it is clear that the JCA model does not capture the effects of the DE pores, even considering the error bars on the prediction; by contrast, the present model with its error bars always includes the experimental curve for the entire frequency band. The theoretical curve calculated from the JCA model in which only a porosity correction is applied shows very interesting results. Indeed, this curve clearly demonstrates that in the frequency range (125–3500 Hz). The effect of the dead end consists mainly in a porosity variation, and both the JCA model with Biot porosity and the present model predict the experimental results fairly well. Above 3500 Hz, the experimental results show that the modified JCA model fails to accurately predict the results. Only the present model, which accounts for both the porosity correction and dead end cavity effect seem able to predict the experimental results.

2. Remark

We should note that it was difficult to test this metallic foam in a classical impedance tube for higher frequencies without changing the DE parameters of metallic foam. Indeed, with respect to the plane wave propagation in the classic impedance tube in order to test higher frequencies, the sample cross-section diameter would have to be smaller. The homogenized principle cannot be strictly applied to the DE pores in the transversal cross-sections.

Generally, the present model improves the comparison with experimental results for a part of all of the tested

aluminum foams. However, for certain foam samples, the proportion of the DE porosity is weak and the DE effect on the sound absorption and sound transmission loss is low (i.e., modifications are on the order of the estimation errors of the DE parameters). Moreover, more research and experiments on a greater number of samples are necessary in order to improve the experimental methods and to more precisely define the two DE parameters.

IV. CONCLUSIONS

In this study, the acoustic properties of materials with dead-end (DE) porosity were examined and, in particular, a certain class of metallic foams. For these materials, the classical fluid model predictions such as the Johnson-Champoux-Allard model are not as satisfying as for other materials.

From a microscopic analysis of dead end pores, a simple model that offers a correction taking this complex microgeometry into account was proposed. After a homogenization process, two acoustic transfer matrix approaches were investigated: one for the non-symmetric DE element, and the second for the symmetric DE element. It appears that the symmetric matrices modeling encompasses the non-symmetric modeling and is therefore, more general.

To validate this model, materials with well controlled parameters, and including DE pores ("simplified samples") were tested. With the use of an impedance tube and the two- and three-microphone technique, the coefficients of absorption and transmission loss were measured. It was found that the comparison between the present model and the experimental results is in much better agreement and the importance of accounting for the DE porosity is noted. Measurements on metallic foams show that an improvement on the theoretical predictions can be obtained with this correction. Analysis of the transmission loss shows the two effects of the two DE parameters on the acoustic indicators. However, for certain metallic foams, the influence of the DE porosity introduces modifications on the order of estimation errors on these parameters and thus, does not allow for definite conclusions.

It is important to develop new theoretical and experimental research on the homogenized criterion and on the two new macroscopic parameters, l_{DE} and ϕ_{DE} (for example: micro-tomography, ultrasonic characterization, comparison of different ϕ measurements, and theoretical study of these materials in bottom-up approaches). It is also necessary to refine the methods of the evaluation of the JCA parameters (notably α_∞, Λ, Λ') and to reduce the uncertainty of the measurements. These new works have to be developed in order to answer the question of whether a material with a complex microstructure can be modeled as one with equivalent dead end pores.

[1]X. L. Gong, Y. Liu, S. Y. He, and J. Lu, J. Mater. Sci. Technol, **20**, 65 (2004).
[2]J. F. Allard and N. Atalla, *Propagation of Sound in Porous Media: Modelling Sound Absorbing Materials* (Wiley and Sons. Ltd., New York, 2009).
[3]J. F. Allard, P. Herzog, D. Lafarge, and M. Tamura, Applied Acous. **39**(1-2), 3 (1993).
[4]Y. Champoux and J. F. Allard, J. Appl. Phys. **70**, 1975 (1991).
[5]T. Bourbié, O. Coussy, and B. Zinsner, Acoustics of Porous Media (Technip, Paris, 1986).
[6]C. Zwikker and C. W. Kosten, *Sound Absorbing Materials* (Elsevier, New York, 1949).
[7]J. Bear, *Hydraulics of Groundwater* (McGraw-Hill, New York, 1979).
[8]I. Fatt, Trans. Am. Inst. Min., Metall. Pet. Eng. **216**, 449 (1959).
[9]R. C. Goodknight, W. A. Klikoff, and I. Fatt, J. Phys. Chem. **64**(9), 1162 (1960).
[10]W. Rose, H. C. Tung, and C. Newman, J. Phys. Chem. **65**(8), 1440 (1961).
[11]R. Goodknight and I. Fatt, J. Phys. Chem. **65**, 1709 (1961).
[12]I. Fatt, Sci. **134**, 1750 (1961).
[13]P. Gibb, M. J. Barcelona, J. D. Ritchey, and M. H. LeFaivre, "Effective porosity of geologic material–First annual report," Report for State Water Survey Division–Illinois department of Energy and Natural Ressources, September 1984.
[14]J. Z. Qian, Z. Chen, H. B. Zhan, and S. H. Luo, Int. J. Rock Mech. Min. Sci. **48**, 132 (2011).
[15]J. Hrabe, S. Hrabetova, and K. Segeth, Biophys.l J. **87**, 1606 (2004).
[16]F. Chevillotte, C. Perrot, and R. Panneton, J. Acoust. Soc. Am. **128**(4), 1766(2010).
[17]P. Leclaire, T. Dupont, O. Sicot, and X. L. Gong, Proceedings Congrès Français d'Acoustique, Lyon, France, April 2010.
[18]K. V. Horoshenkov and M. J. Swift, J. Acoust. Soc. Am. **110**, 2371 (2001).
[19]D. T. Blackstock, *Fundamentals of Physical Acoustics* (Wiley and Sons Inc., New York, 2000).
[20]M. A. Biot, J. Acoust. Soc. Am. **28**, 168 (1956).
[21]M. A. Biot, J. Acoust. Soc. Am. **28**, 179 (1956).
[22]D. L. Johnson, J. Koplik, and R. Dashen, J. Fluid Mech. **176**, 379 (1987).
[23]R. Panneton, J. Acoust. Soc. Am. **122**(6), EL217 (2007).
[24]ISO-10534-2, "Acoustics—Determination of sound absorption coefficient and impedance in impedance tubes. Part 2: Transfer-function method," International Organization for Standardization, Geneva, Switzerland, 1998.
[25]Y. Salissou, R. Panneton, and O. Doutres, "Three-microphone method for measuring the normal sound transmission loss of noise control samples in standing wave tube," Appl. Acoust. (submitted).
[26]M. R. Stinson and G. A. Daigle, J. Acoust. Soc. Am. **83**, 2422 (1988).
[27]Y. Salissou and R. Panneton, J. Appl. Phys. **101**, 124913.1 (2007).
[28]P. Leclaire, L. Kelders, W. Lauriks, C. Glorieux, and J. Thoen, J. Acoust. Soc. Am. **99**, 1944 (1996).
[29]B. Brouard, B. Castagnède, M. Henry, D. Lafarge, and S. Sahraoui, Techniques de l'Ingénieur, **R6**, 120 (2003).
[30]Z. E. A. Fellah, S. Berger, W. Lauriks, C. Depollier, C. Aristegui, and J.-Y. Chapelon, J. Acoust. Soc. Am. **113**(5), 2424 (2003).
[31]F. Fohr, D. Parmentier, B. Castagnède, and M. Henry, in *Proceedings of Acoustics'08*, Paris, France, 30 June–4 July 2008.